Geoderma 315 (2018) 75–87

Contents lists available at ScienceDirect

Geoderma

journal homepage: www.elsevier.com/locate/geoderma

Understanding saturated hydraulic conductivity under seasonal changes in climate and land use

Mohamed Elhakeem[a], A.N. Thanos Papanicolaou[b,*], Christopher G. Wilson[b], Yi-Jia Chang[c], Lee Burras[d], Benjamin Abban[b], Douglas A. Wysocki[e], Skye Wills[e]

[a] Abu Dhabi University, Civil Engineering Department, Abu Dhabi, P.O. Box 59911, United Arab Emirates
[b] University of Tennessee, Hydraulics & Sedimentation Laboratory, Department of Civil & Environmental Engineering, Knoxville, TN 37996, USA
[c] DGR Engineering, Rock Rapids, IA 51246, USA
[d] Iowa State University, Department of Agronomy, Ames, IA 50011, USA
[e] USDA-NRCS National Soil Survey Center, Lincoln, NE 68508, USA

ARTICLE INFO

Handling Editor: Morgan Cristine L.S.

Keywords:
Saturated hydraulic conductivity
Pedotransfer functions
Watershed models
Geographic Information System

ABSTRACT

The goal of this study was to understand better the co-play of intrinsic soil properties and extrinsic factors of climate and management in the estimation of saturated hydraulic conductivity (K_{sat}) in intensively managed landscapes. For this purpose, a physically-based, modeling framework was developed using hydro-pedotransfer functions (PTFs) and watershed models integrated with Geographic Information System (GIS) modules. The integrated models were then used to develop K_{sat} maps for the Clear Creek, Iowa watershed and the state of Iowa. Four types of saturated hydraulic conductivity were considered, namely the baseline (K_b), the bare (K_{br}), the effective with no-rain ($K_{e\text{-}nr}$) and the effective (K_e) in order to evaluate how management and seasonality affect K_{sat} spatiotemporal variability. K_b is dictated by soil texture and bulk density, whereas K_{br}, $K_{e\text{-}nr}$, and K_e are driven by extrinsic factors, which vary on an event to seasonal time scale, such as vegetation cover, land use, management practices, and precipitation. Two seasons were selected to demonstrate K_{sat} dynamics in the Clear Creek watershed, IA and the state of Iowa; specifically, the months of October and April that corresponded to the before harvesting and before planting conditions, respectively.

Statistical analysis of the Clear Creek data showed that intrinsic soil properties incorporated in K_b do not reflect the degree of soil surface disturbance due to tillage and raindrop impact. Additionally, vegetation cover affected the infiltration rate. It was found that the use of K_b instead of K_e in water balance studies can lead to an overestimation of the amount of water infiltrated in agricultural watersheds by a factor of two. Therefore, we suggest herein that K_e is both the most dynamic and representative saturated hydraulic conductivity for intensively managed landscapes because it accounts for the contributions of land cover and management, local hydropedology and climate condition, which all affect the soil porosity and structure and hence, K_{sat}.

1. Introduction

Saturated hydraulic conductivity (K_{sat}), or when the infiltration rate reaches steady state (e.g., Smith, 2002; McCuen, 2003), is a key, dynamic property for assessing the impacts of climate and management on the behavior of soil and water (e.g., Papanicolaou et al., 2015; Elhakeem et al., 2017). K_{sat} is often used in soil interpretations, hydropedological catena assessments across landscapes, and physically based modeling exercises to determine water budgets, water-plant relationships, soil suitability for agriculture, and leaching potential (Nearing et al., 1996; Arnold et al., 1998; Lin, 2003; Schoeneberger and Wysocki, 2005; West et al., 2008).

However, K_{sat} exhibits a nonlinear behavior in response to external forcings resulting in high spatiotemporal variability at both large and small scales. This complex response is due to the co-play of different intrinsic soil properties, such as texture and bulk density, and extrinsic factors, including land use, vegetation cover, and precipitation (Gupta et al., 1996; Webster and Oliver, 2001; Papanicolaou et al., 2008; Elhakeem and Papanicolaou, 2009; Safadoust et al., 2012). The intrinsic soil properties mostly dictate the spatial variability of K_{sat}, while the added temporal variability of K_{sat} is due to the extrinsic factors (Alleto and Coquet, 2009; Elhakeem and Papanicolaou, 2012).

Capturing this spatiotemporal variability in K_{sat} is challenging as instruments, such as double ring infiltrometers, are labor-intensive and

* Corresponding author.
E-mail address: tpapanic@utk.edu (A.N.T. Papanicolaou).

https://doi.org/10.1016/j.geoderma.2017.11.011
Received 6 September 2017; Received in revised form 19 October 2017; Accepted 5 November 2017
Available online 08 December 2017
0016-7061/

expensive. Several spatially distributed point measurements that are conducted for long periods are necessary to measure the spatial and temporal variability of K_{sat} (Papanicolaou et al., 2008). Semi-automation of these instruments has helped ease the load (e.g., Papanicolaou et al., 2015). Yet, performing enough detailed, continuous measurements with the semi-automated instruments remains a daunting task, even in small hillslope-scale studies (10^3–10^5 m^2).

Implicit methods for estimating K_{sat} to address the spatial and temporal limitations related to in-situ measurements include the use of infiltration and watershed models coupled with geospatial tools (Mohatny, 2013). Needless to say, some field measurements are still necessary at representative sites for methods validation.

Several, semi-empirical, infiltration models (i.e., pedotransfer functions, PTFs) exist that estimate saturated hydraulic conductivity based on the correspondence between K_{sat} and intrinsic soil properties, such as texture and bulk density (Schaap, 1999; Ferrer Julia et al., 2004; Rezaei Arshad et al., 2013; Patil and Singh, 2016). K_{sat} estimates that only consider intrinsic soil properties provide a *baseline* saturated hydraulic conductivity, K_b, across space. Most K_{sat} estimates reported in public databases (e.g., NCSS, UNSODA, WISE, HYPRES) are baseline values (e.g., Leenhardt et al., 1994; Leij et al., 1996; Schaap and Leij, 1998; Wosten et al., 1999; Lin et al., 2014).

Watershed models adjust K_b values by considering extrinsic factors such as vegetation cover, land use, management practices, and precipitation, which vary on an event to seasonal time scale (e.g., Nearing et al., 1996; Arnold et al., 1998; Ju et al., 2010). The K_{sat} estimates that consider both the intrinsic and extrinsic factors provide an *effective* hydraulic conductivity, K_e (Paleologos et al., 1996; Deb and Shukla, 2012). In essence, K_e is a "corrected form" of K_b which accounts for climate seasonality and land use change. The models convert "static" K_b values into "dynamic" K_e values, thus making them more pertinent for watershed management.

The objective of this study was to understand better the co-play of intrinsic soil properties and extrinsic factors of climate and management in K_{sat} dynamics through the development of a physically based, geospatial modeling framework to estimate K_{sat} at the watershed scale and larger. The framework presented here integrates regionally representative PTFs, physically based watershed models, and Geographic Information System (GIS) modules to quantify four different K_{sat} types that reflect the influences of both the intrinsic properties and extrinsic factors. The framework estimates the following four types of saturated hydraulic conductivity: (1) the baseline hydraulic conductivity, K_b, that accounts for the intrinsic soil properties; (2) the bare saturated hydraulic conductivity, K_{br}, that adjusts K_b for the effects of soil crusting; (3) the effective saturated hydraulic conductivity with no-rain, $K_{e\text{-}nr}$, that adjusts K_{br} for the effects of vegetation cover; and ultimately, (4) the effective saturated hydraulic conductivity, K_e, that adjusts $K_{e\text{-}nr}$ for the effects of individual rainfall events, which makes it the most dynamic type among the four.

The modeling framework was established first in a representative, intensively managed watershed of the U.S. Midwest, Clear Creek, Iowa where detailed K_{sat} measurements exists (Papanicolaou et al., 2015). Then, the framework was extended to quantify K_b, K_{br}, $K_{e\text{-}nr}$, and K_e for the entire state of Iowa. Maps of the four K_{sat} types were developed for Clear Creek and Iowa for two time periods, October and April corresponding to the pre-harvest and pre-planting conditions, respectively. These maps demonstrate both the spatial and temporal variability of K_{sat} due to changes in soil properties, climate, and management. In addition, a statistical analysis and histograms were provided for the four types and comparisons are made to discern the effect of the extrinsic factors on K_{sat} dynamics.

2. Modeling framework development

2.1. Model selection

The first step towards developing the modeling framework was to select the appropriate PTF and watershed model based on physical reasoning and model performance (Vieux, 2004). The chosen PTF and model should adequately represent site conditions and capture the dynamicity of K_{sat} induced by climate and land management.

The estimates provided by the PTFs and models were compared using seven statistical criteria to direct K_{sat} measurements in selected fields of the test watershed, Clear Creek (Papanicolaou et al., 2015). These criteria included the mode, minimum, maximum, root mean square error, Akaike Information Criterion, geometric mean error ratio, and geometric standard deviation of the error ratio.

The mode was used to examine the symmetry of the observed and estimated values around the mean. The minimum and maximum evaluated the agreement between the ranges of the observed and estimated values.

The root mean square error is a quadratic scoring criterion, which measures the average magnitude of the error in the model estimates. The Akaike Information Criterion is a goodness-of-fit measure of a regression model that tries to minimize the model complexity by imposing a penalty for increasing the number of coefficients (Akaike, 1974; Bozdogan, 1987). For both the root mean square error and the Akaike Information Criterion, lower values indicate better performance of the model. A perfect agreement between the measured and estimated values is satisfied when $RMSE = 0$ and $AIC = 2k$, where k is the number of coefficients used in the model.

The geometric mean error ratio and standard deviation of the error ratio account for the log-tailed distribution of K_{sat} (Tietje and Richter, 1992; Papanicolaou et al., 2015). Perfect agreement between the estimated and the measured values is obtained when these values equal 1.0.

To evaluate the overall performance of the PTFs and models (Table 1), relative scores on a linear scale between 0 and 1 were assigned for each of the aforementioned criterion based on the degree of agreement between the measured and estimated values, and then summed (Shahin et al., 1993). The Rosetta PTF that considers bulk density (i.e., Rosetta - BD), as well as the Water Erosion Prediction Project (WEPP) model provided the closest agreement to the measured K_{sat} in Clear Creek and were incorporated into the modeling framework for this study. Papanicolaou et al. (2015) found that the bulk density dominated the infiltration process in soils experiencing the effects of compaction due to agricultural activity as it alters the soil porous network. Additionally, the WEPP PTFs capture the effects of management through changes in roughness and cover. Brief descriptions of Rosetta and WEPP, in the context of the modeling framework are given in following section.

2.2. Description of models

Rosetta is a modeling platform that estimates water retention parameters, as well as unsaturated and saturated hydraulic conductivity (Schaap et al., 1998, 2001). These parameters are determined using PTFs with various orders of complexity that incorporate sand, silt, and clay percentages, as well as bulk density and water retention points as model inputs. Therefore, it provides values for K_b.

WEPP is a physically based, spatially distributed, watershed model that estimates surface runoff and erosion from agricultural fields under different land uses and management practices (Flanagan et al., 1995, 2007). More detailed descriptions of WEPP and its applications are provided elsewhere (Alberts et al., 1995; Ascough et al., 1994; Abaci and Papanicolaou, 2009; Dermisis et al., 2010; Papanicolaou et al., 2017a).

WEPP can simulate the four K_{sat} types for different hillslopes on an

Table 1
PTFs and watershed models performance.

Criterion[a]		Mode	Min.	Max.	*AIC*	*RMSE*	*GMER*	*GSDER*	Total	Ω (%)
PTF	Cosby et al. (1984)	0.80	0.82	0.18	0.85	0.89	0.60	0.71	4.85	69
	Brakensiek et al. (1984)	0.87	0.98	0.42	0.54	0.68	0.36	0.71	4.56	65
	Saxton et al. (1986)	0.85	0.97	0.40	0.51	0.66	0.39	0.72	4.50	64
	Rawls and Brakensiek (1985)	0.32	0.72	0.23	0.96	0.95	0.89	0.86	4.93	70
	Vereecken et al. (1990)	0.02	0.02	0.37	0.35	0.47	0.02	0.14	1.40	20
	Jabro (1992)	0.73	0.94	0.08	0.21	0.15	0.10	0.65	2.86	41
	Dane and Puckett (1994)	0.51	0.68	0.37	0.93	0.93	0.83	0.78	5.03	72
	Campbell and Shiozawa (1994)	0.74	0.91	0.03	0.12	0.10	0.02	0.53	2.45	35
	Risse et al. (1995)	0.85	0.92	0.12	0.33	0.42	0.09	0.50	3.23	46
	Wosten et al. (1999)	0.83	0.91	0.42	0.66	0.81	0.61	0.55	4.79	68
	Rosetta BD – Schaap (1999)	0.59	0.83	0.79	0.79	0.91	0.93	0.76	5.60	**80**
	Rosetta – Schaap (1999)	0.91	0.72	0.17	0.73	0.88	0.67	0.78	4.86	69
WSM	KINEROS (Smith et al., 1995)	0.67	0.53	0.18	0.88	0.88	0.58	0.69	4.41	63
	WEPP (Nearing et al., 1996)	0.86	0.98	0.38	0.99	0.97	0.92	0.84	5.94	**85**
	CAESAR (Coulthard et al., 2002)	0.35	0.89	0.28	0.88	0.88	0.58	0.69	4.55	65

The numbers in bold text signify the PTF and watershed model with the highest rankings.
[a] $AIC = N(Ln(2\pi\Sigma_{i=1}^{N}(O_i - P_i)^2/N) + 1) + 2k$, $RMSE = \sqrt{(1/N)\sum_i^N (O_i - P_i)^2}$, $GMER = \exp((1/N)\Sigma_{i=1}^{N} Ln(P_i/O_i))$, $GSDER = \exp[((1/(N-1))\Sigma_{i=1}^{N}(Ln(P_i/O_i)/GMER)^2)^{1/2}]$, where N = sample size, O_i = observed values, P_i = predicted values, k = the number of parameters in the models. Ω = the overall performance in percentage, BD = the bulk density.

event basis considering different landscape attributes, climate, land use, and management (Nearing et al., 1996; Flanagan et al., 2007). Although WEPP does provide K_b values, the PTF of Rosetta - BD was used herein due to its incorporation of bulk density. Bulk density, as it relates to compaction from farming activities, was a controlling factor of K_{sat} in agricultural fields (e.g., Mudgal et al., 2010; Papanicolaou et al., 2015). The Rosetta-BD K_b values were then passed to WEPP to calculate the bare hydraulic conductivity (K_{br}) that accounts for the formation of soil crusts, which can inhibit infiltration (Risse et al., 1995).

K_{br} accounts for this crusting as follows (Risse et al., 1995):

$$K_{br} = K_b[\mathrm{CF} + (1 - \mathrm{CF})e^{-C \cdot E_a(1 - RR_t/RR_{r-max})}] \quad (1)$$

where *CF* is the crust factor, *C* is soil stability factor, E_a is the cumulative rainfall kinetic energy since the last tillage, RR_t is the random roughness height, and $RR_{t\text{-}max}$ is the maximum random roughness height. The *CF* is a function of the capillary potential at the crust/sub-crust interface, partial saturation of the sub-crust soil, and the wetting front depth with typical values ranging from 0.2 to 1.0 (e.g., Morin et al., 1989). Soil crusts result from broken-down aggregate fragments that infiltrate into soil pores, causing the pores to clog. Additionally, the clays and sands mix forming a cement-like crust as the soil dries reducing the permeability of soil (Papanicolaou et al., 2017b). However, different soil textures and higher soil roughness can limit the crusting effect (Rawls and Brakensiek, 1985). Like *CF*, the soil stability factor is a function of soil properties (e.g., texture and cation exchange capacity) with reported values between 0.0001 and 0.01 (Bosch and Onstad, 1988; Burras et al., 2005). The cumulative rainfall kinetic E_a since the last tillage is estimated from Salles et al. (2002). RR_t reaches a maximum (i.e., $RR_{t\text{-}max}$) of about 40 mm immediately after tillage and then decreases exponentially with time (Potter, 1990).

$K_{e\text{-}nr}$ is the effective hydraulic conductivity, which is determined without rainfall, builds on the bare condition by considering cover. K_e further considers how the precipitation amount from an individual rain event can alter K_{sat}:

$$K_{e-nr} = K_{br}(1 - C_{TE}) \quad (2)$$

$$K_e = K_{br}(1 - C_{TE}) + (0.0534 + 0.01179K_b)C_{TE}P \quad (3)$$

where P is the storm rainfall amount in mm and C_{TE} is the total effective surface cover partitioning the fractions of the canopy and residue. This is the last step in the WEPP estimation of K_{sat} where both intrinsic and extrinsic factors have been considered.

2.3. Model integration with GIS

Rosetta v. 1.2 and WEPP v. 2012.8 were loosely linked with ArcGIS v. 9.3.1 (Environmental Systems Research Institute, ESRI, Redlands, CA) to develop a physically-based, modeling framework within which different pedological, climatic, and land use data were incorporated. The modeling framework provides visualizations of K_{sat} in the form of daily geospatial maps that change as the extrinsic factors change (e.g., Ju et al., 2010).

Geospatial data for both Rosetta and WEPP were obtained from open-access Internet sources and compiled using a FORTRAN v. 2008 algorithm (Chang, 2010). In this algorithm, registries of data and computational resources were developed using XML files to allow for automatic input of different geographically distributed data sources through web interfaces. The data were downloaded in a format that was easily implemented into a GIS platform. Layered information of soil, vegetation, random roughness, and precipitation obtained from the geospatial and remote sensing databases were combined and polled to provide the appropriate information for different models. The ArcMap extension converted the soil vector maps into raster maps of the different variables, and the data points from the raster maps were used for statistical analysis.

3. Implementation of models

3.1. Study site

Clear Creek (Fig. 1a) is representative of Iowa and to a degree most of the Midwest in terms of land use (predominantly agricultural with developing small pockets of urban areas), soil (Alfisols and Mollisols), and climate (humid-continental). With a total drainage area of 270 km^2, it drains directly to the Iowa and ultimately the Mississippi Rivers.

The watershed is part of the U.S. National Science Foundation, Intensively Managed Landscapes-Critical Zone Observatory (IML-CZO; http://criticalzone.org/iml). The IML-CZO has available hydrologic, erosion, biogeochemical, management, and economic databases for educating models. Additional data from remote sensing sources were also used to look at information from the watershed scale.

The dominant soils in Clear Creek are Mollisols with Alfisols also present but to a lesser extent (United States Department of Agricultural-USDA, 2008). The most common soil associations are the Tama-Downs,

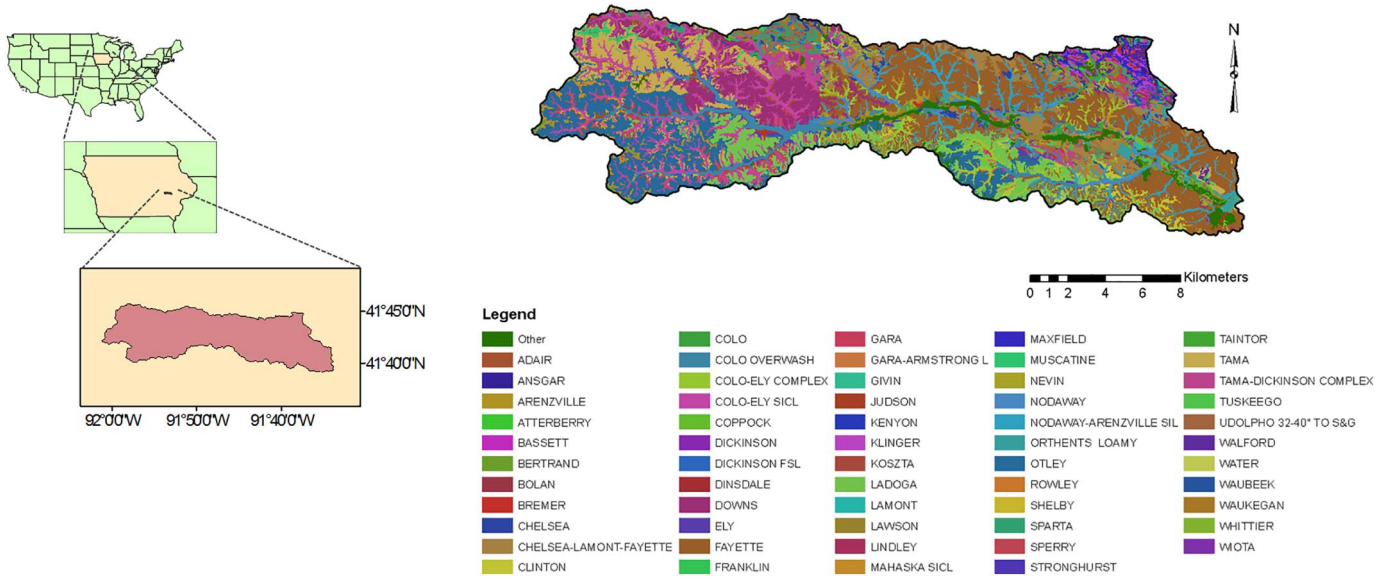

Fig. 1. The study site: (a) The Clear Creek watershed, IA; (b) a soil map of the watershed from the Iowa County Soil Survey.

Fayette-Downs, and Colo-Nevin-Nodaway associations (Fig. 1b). The Tama-Downs and Fayette-Downs upland soils are well drained and formed on a prairie-savannah-forest biosequence (Dideriksen et al., 2007). The Colo-Nevin-Nodaway soil association formed on stream terraces and flood plains. The drainage classes range from poorly drained to moderately well drained (Highland and Dideriksen, 1967).

Over 80% of the watershed has been converted from the prairie-savannah-forest biome to row-crop agriculture and pasture (Rayburn and Schulte, 2009). Since 1991, the dominant management strategies in the watershed are corn-soybean rotations that use conservation tillage practices (reduced and no-till). Restored forests and grasslands, as well as urban areas comprise the remaining land uses.

Due to the mid-continental location of Iowa, Clear Creek climate is characterized by hot summers, cold winters, and wet springs (Highland and Dideriksen, 1967). Summer months are influenced by warm, humid air masses from the Gulf of Mexico, while dry Canadian air masses dominate the winter months. Average daily temperature is about 10 °C, ranging from an average July maximum of 29 °C to an average January minimum of −13 °C. Mean annual precipitation is approximately 889 mm with convective thunderstorms prominent in the summer, and snowfall in the winter, which averages 762 mm annually. The growing season lasts about 180 days in Southeast Iowa.

3.2. Inputs and data sources of models

Table 2 summarizes the input variables for estimating K_b, K_{br}, $K_{e\text{-}nr}$, and K_e, which include soil, land use, and precipitation data. The soils data were obtained from the Iowa Soil Properties And Interpretations Database (ISPAID; https://www.extension.iastate.edu/soils/ispaid). The database provides information regarding the taxonomic classification (e.g., order; suborder; series), hydrologic soil group, texture, bulk density, organic matter, cation exchange capacity, and soil pH. The soil information in the database was confirmed with soil cores collected in Clear Creek (Oneal, 2009).

Light Detection And Ranging (LiDAR) data were obtained through the IML-CZO (http://data.imlczo.org/) from the Agricultural Conservation Planning Framework Development Team at the USDA/ARS National Laboratory for Agriculture and the Environment (http://www.gis.iastate.edu/gisf/projects/acpf). The LIDAR data provided elevations with an error of 20 cm. Detailed land use and management information for Clear Creek was provided from the IML-CZO.

The Hydro-NEXt-generation RADar (NEXRAD)-estimated precipitation depth and intensity were obtained from the Iowa Environmental Mesonet (IEM; https://mesonet.agron.iastate.edu/) of the Department of Agronomy at the Iowa State University and compared to the tipping bucket data in Clear Creek. The deviation between the radar and tipping bucket data was less than 10%.

Table 2
Model inputs and range of the variables in Clear Creek watershed.

K_{sat}	Input variables	Unit	Maximum	Minimum
K_b	% Sand (Sa)	Percent	86	3
	% Clay (Cl)	Percent	36	6
	Bulk density (BD)	Kg/m^3	1.53	1.27
K_{br}	K_b	mm/h	83.6	2.5
	Cation exchange capacity (CEC)	meq/100 g	39	0
	Crust factor (CF)	Dimensionless	0.5378	0.4324
	Soil stability factor (C)	m^2/J	0.00786	0.0001
	Random roughness (RR_t)	m	0.04	0.01
	Cumulative rainfall kinetic energy (E_a) for May 2007 to October 2007	kJ/m^2	13.2	9.8
	Cumulative rainfall kinetic energy (E_a) for November 2007 to April 2008	kJ/m^2	6.1	4.6
K_e	Precipitation (P) for 10/17/2007	mm	48.8	36.6
	Precipitation (P) for 4/18/2008	mm	34.8	20.8
	Total effective cover (C_{TE}) for October	Fraction	1	0
	Total effective cover (C_{TE}) for April	Fraction	1	0
	K_{br} for October 2007	mm/h	42.8	1.3
	K_{br} for April 2008	mm/h	42.8	1.3

4. Results

Dynamic maps of the four K_{sat} types were developed using the coupled Rosetta-WEPP-GIS modeling framework for Clear Creek. The results focus on two specific periods (October 2007 and April 2008) that correspond to the K_{sat} field measurements in Clear Creek used for model verification. Additionally, these periods highlight the seasonal variability of K_{sat} due to changes in climate (i.e., rainfall intensity) and land management (i.e., the effects of residue and crop cover). The maps were complemented with histograms and statistical analysis to understand the co-play among the intrinsic properties and extrinsic factors governing K_{sat} dynamics.

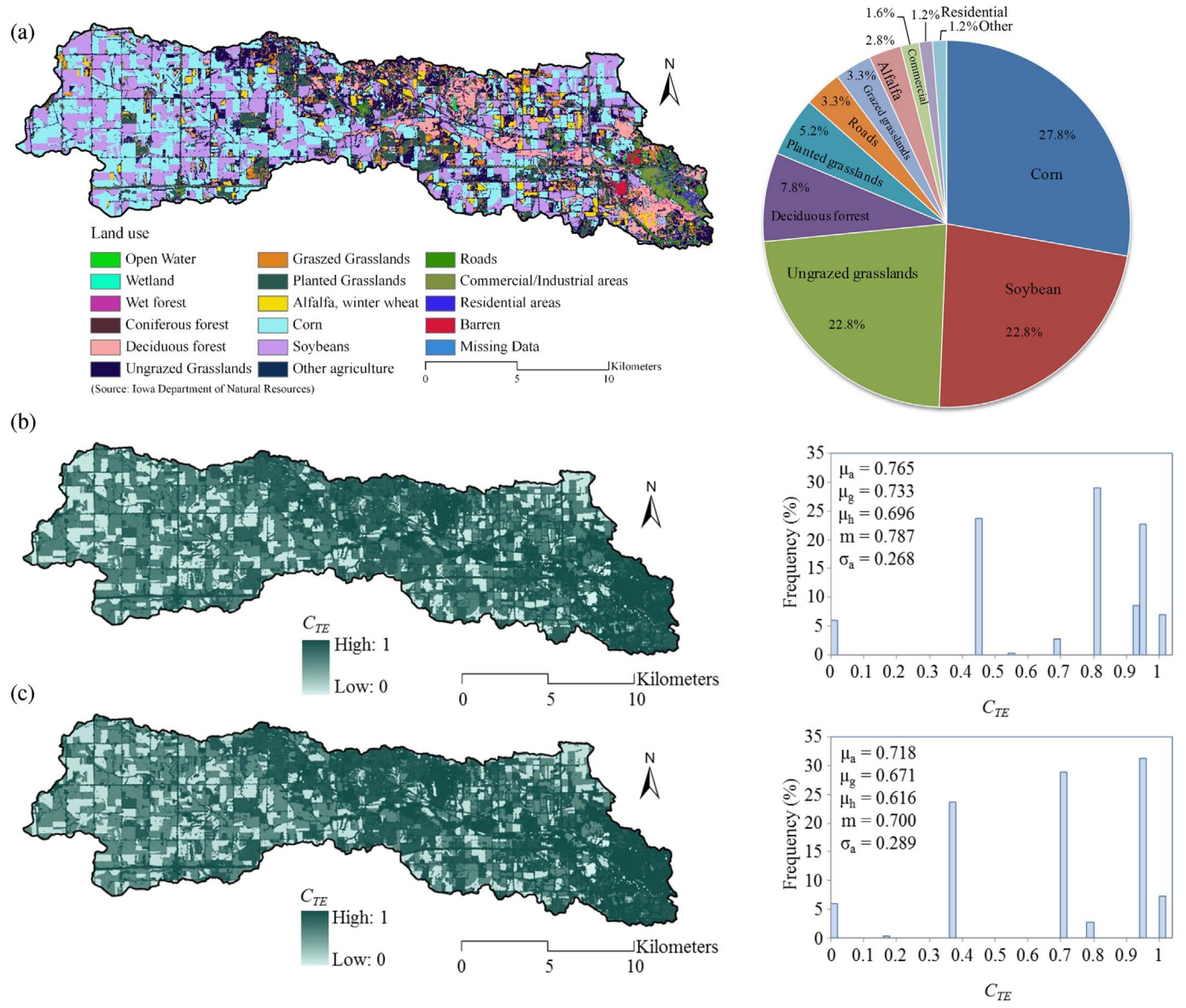

Fig. 2. Maps and histograms of Clear Creek land uses and total effective cover (CTE): (a) Land uses from the National Land Cover Database; (b) Total effective cover in October 2007; (b) Total effective cover in April 2008.

4.1. Model key input variables

The dynamics of K_{sat} are primarily related to the effects of climate and management. Specifically in the equations for K_{br}, $K_{e\text{-}nr}$, and K_e, the key input variables include the total effective cover, C_{TE}; the cumulative rainfall kinetic energy, E_a; and total event rainfall, P.

Since C_{TE} is a function of both canopy and residue cover, it reflects changes over the crop life cycle, or the growing season. The C_{TE} values were estimated using a detailed land use classification map (Fig. 2a) from the National Land Cover Database, as well as the vegetation and management practices databases of WEPP. Fig. 2b and c, respectively, show maps of the C_{TE} for Clear Creek during two periods that bracket the growing season, October 2007 (pre-harvest) and April 2008 (pre-planting). The histograms of C_{TE} for the two months adjacent to the maps in Fig. 2b and c show the median (m); the arithmetic (μ_a), geometric (μ_g), and harmonic (μ_h) means; and the arithmetic (σ_a) and geometric (σ_g) standard deviations. The relatively large standard deviations are attributed to the land use diversity in Clear Creek, which includes forest, agricultural, grasslands, and residential areas. The zero values in the histograms refer to streams, ponds, and lakes in the watershed. Both maps show high C_{TE} values (0.70–0.95) in the north-central and southeastern parts of the watershed. The re-established deciduous forests and prairies in the F.W. Kent Park (maintained by the Johnson County, IA Soil & Water Conservation Board) are in the north-central part, while the residential areas of Tiffin and Coralville sit in the southeastern part of the watershed. In these areas, the C_{TE} values change very little across the growing season due to the more permanent cover.

In contrast, C_{TE} values for the corn-soybean fields vary year to year as corn has higher C_{TE} values than soybeans. Corn and soybeans had average C_{TE} values of 0.75 and 0.37, respectively. There was little change in the C_{TE} values for each crop over the growing season, though. C_{TE} is calculated as the sum of the residue and canopy cover. In October, the fields had predominantly canopy cover as the crops were mature, but very low residue cover. In April, the fields had high residue cover, as most framers practice a reduced tillage in the watershed. October had slightly higher C_{TE} values than April, which indicates that canopy cover was more abundant than the residue cover.

Fig. 3 shows the representative maps and histograms of the rainfall (E_a and P) data in Clear Creek. Fig. 3a and b show maps of the rainfall

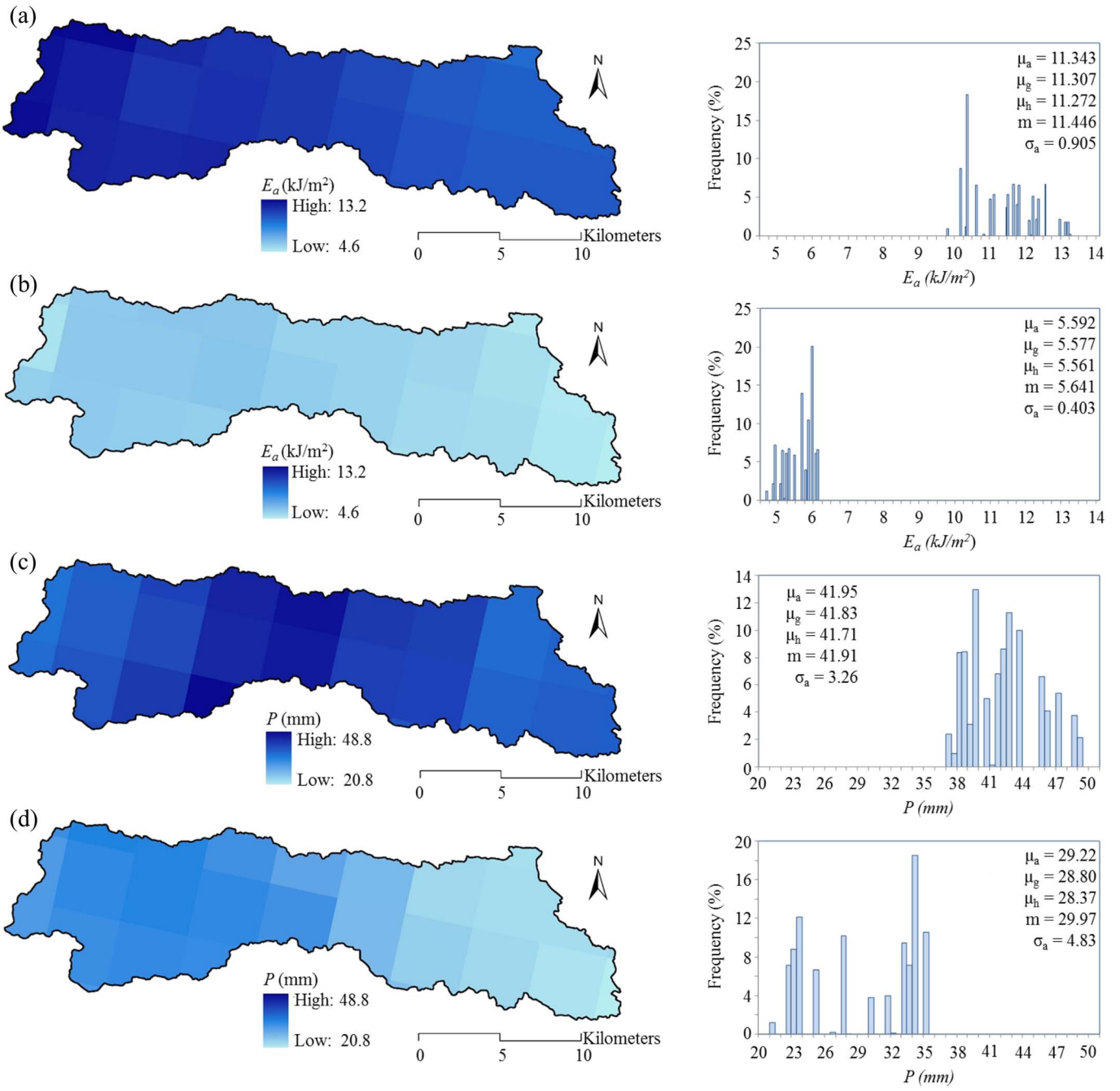

Fig. 3. Maps and histograms of rainfall data in Clear Creek. (a) Cumulative rainfall kinetic energy distribution from May 2007 to October 2007. (b) Cumulative rainfall kinetic energy distribution from November 2007 to April 2008. (c) Rainfall depth distribution for the single storm event of October 17, 2007. (d) Rainfall depth distribution for the single storm event of April 18, 2008.

cumulative kinetic energy (E_a) since the last tillage for the summer-fall and winter-spring seasons, respectively. The cumulative kinetic energy is summed between tillage events, as the tillage resets the roughness changes caused by the raindrop impact, and hence affects the ability for the soil to form crusts. The maps show higher E_a for the summer-fall (i.e., May–October) season compared to the winter-spring (i.e., November – April) season, as May and June experience intense convective thunderstorms (Wilson et al., 2012). For both periods, the E_a values were higher in the western part of the watershed than in the eastern part, which is most likely a rainout effect as storms tend to move from west to east, losing energy as they progress.

The distribution of E_a was wider in the summer-fall compared to the winter-spring, which agree with trends found in Midwestern watersheds (Dai et al., 2016). For the November–April period, the histograms show a bimodal distribution for the event, with the higher peak associated with the rainfall in the western part of the watershed. Nonetheless, the insignificant differences were signified by small standard deviations.

Fig. 3c and d show the rainfall depths (P) for two selected days during October 2007 and April 2008, considered for illustrating the dynamic effects of P on K_e. These days (October 17, 2007 and April 18, 2008) were the highest rainfall events in the two months and were selected to demonstrate a "maximum" effect of rainfall on K_{sat}. Overall, the October event had higher P values than the April event. In terms of rainfall distribution, the central part of the watershed received the majority of the rainfall during the event, while the April event showed

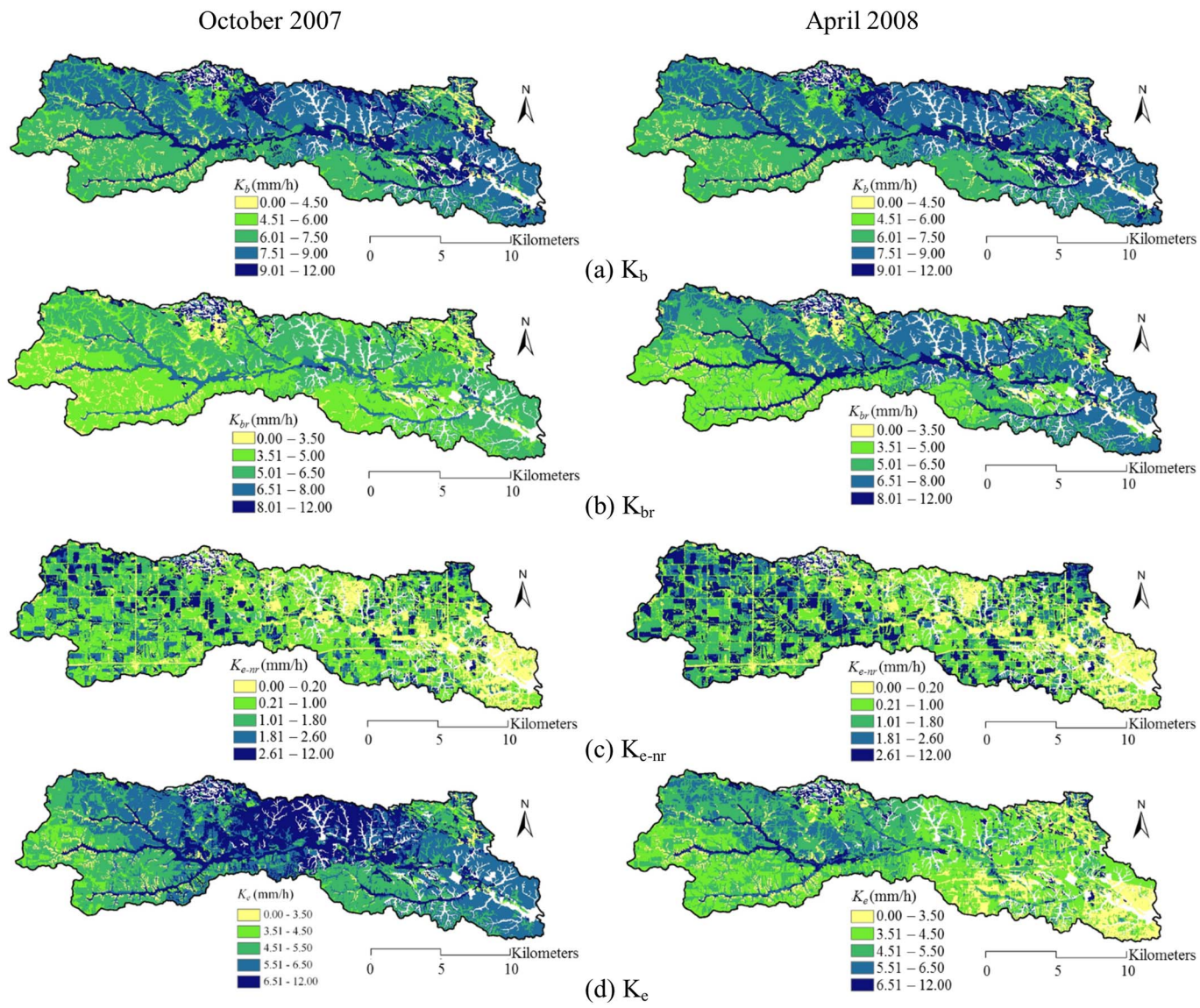

Fig. 4. Maps of the saturated hydraulic conductivity in the Clear Creek: (a) K_b; (b) K_{br}; (c) $K_{e\text{-}nr}$; (d) K_e for the single storm events of October 17, 2007 and April 18, 2008.

more rain over the western part of the watershed. The histograms for P, follow similarly to those of E_a.

4.2. Analysis of the K_{sat} dynamics

The maps in Fig. 4 show the K_b, K_{br}, $K_{e\text{-}nr}$, and K_e in Clear Creek for the two chosen periods. Fig. 4a shows the baseline saturated hydraulic conductivity (K_b) calculated from Rosetta-BD. K_b depends only on "static" soil properties, and it is identical for both periods. For the most part, K_b is higher in the northern part of the watershed compared to the southern part, with the extreme northeast part of the watershed as an exception. The texture in the northern part had lower clay percentages (average = 11%) compared to the southern part (average = 23%).

Fig. 4b shows the bare saturated hydraulic conductivity (K_{br}) maps for Clear Creek for October 2007 and April 2008 calculated with Eq. (1) that is built in WEPP. The K_{br} calculations consider soil crusting and stability, random roughness, and the cumulative rainfall kinetic energy. RR_t and E_a, in particular, are dynamic variables that account for the changes in the management practices and climate conditions, respectively throughout the year.

The RR_t for October and April both averaged 0.01 m, which corresponded to the minimal land surface disturbance effects, as October and April are several months after tillage occurred, which allowed the ground to settle.

The E_a for October 2007 was determined from the precipitation data between May and October 2007. For April 2008 the precipitation data from November 2007 to April 2008 were considered. April had overall higher K_{br} values than October, because K_{br} is inversely proportional to E_a. The most intense rainfall in Clear Creek occurs due to convective thunderstorms in May and June (e.g., Wilson et al., 2012). The inverse relationship between K_{br} and E_a is attributed to the amounts of runoff and erosion. As aggregates breakdown from rain splash or runoff, some of the finer soil particles settle into the soil pores, blocking them. Additionally, the clays and sands mix forming a cement-like crust reducing the permeability of soil, and hence reduce the values of K_{br} (e.g., Eigel and Moore, 1983; Sun et al., 2010; Hu et al., 2012; Sutarto et al., 2014; Papanicolaou et al., 2017b).

Fig. 4c shows the maps of $K_{e\text{-}nr}$ in Clear Creek for October and April. $K_{e\text{-}nr}$ considers only the effect of land cover, see Eq. (2). Both months show lower values of $K_{e\text{-}nr}$ in the north-central and southeastern parts of CCW, which reflect the high values of total effective cover (C_{TE}) and land use in these areas (see Fig. 2). These trends coincide with the land use maps of these parts of the watershed, which are mainly comprised of the restored forests in F.W. Kent Park and residential areas of Tiffin

and Coralville. Thus, there were no significant changes in $K_{e\text{-}nr}$ values at these areas due to seasonal differences.

When comparing the $K_{e\text{-}nr}$ values in the row crop areas of the watershed, corn fields had lower $K_{e\text{-}nr}$ values than the soybean fields, because the corn had a higher C_{TE} as corn plants have higher biomass over soybean plants (Abaci and Papanicolaou, 2009; Diiwu et al., 1998). However, there were no significant changes in the $K_{e\text{-}nr}$ values due to seasonal differences in the same field.

Maps of K_e, which have the additional term in Eq. (3) accounting for the effects of single storm events, are shown in Fig. 4d. The maps are plotted for the days of the highest rainfall events in October 2007 and April 2008 to demonstrate a "maximum" effect of a single rainfall event on K_e. For the October event, K_e values were higher at the central part of the watershed, while for the April event the K_e values were higher at the western part. This is attributed to the rainfall distribution over the watershed during these two days (see Fig. 2). Because K_e is linearly proportional to rainfall depth (e.g., Hardie et al., 2013) and the October event had higher precipitation than the April event, overall the maps show higher K_e for the single storm event of October 17, 2007 compared to the event on April 18, 2008. The proportional relationship between K_e and rainfall depth is attributed to the fact that for higher precipitation it is more likely to break the protective crust layer, thereby allowing for higher infiltration rates. Elhakeem and Papanicolaou (2012) has shown that a positive correlation exists between K_e and event rainfall depth.

Fig. 5 shows the histograms and the statistical measures obtained from the K_{sat} maps. The histograms for each K_{sat} types have unique patterns that do not vary significantly between the periods. Only the magnitude of the median is shifted due to the seasonal effect. The histograms of K_b and K_{br} are bimodal. In contrast, the histogram of $K_{e\text{-}nr}$ is positively skewed, whereas the histogram of K_e is almost symmetric.

The geometric mean (μ_g) and median (m) are more representative of the various saturated hydraulic conductivity distributions due to their wide ranges. Comparisons using the median between the relative magnitudes of K_b, K_{br}, $K_{e\text{-}nr}$, and K_e show that K_b was higher compared to the other K_{sat} types for both months. Thus, K_b, is essentially a maximum potential K_{sat} value that must be corrected to account soil, cover, climate, and management factors.

The histograms of K_{br} show a decrease of about 30% relative to K_b emphasizing the important role that cumulative rainfall kinetic energy (E_a) and management practices and their effects on aggregate breakdown play on saturated hydraulic conductivity (Khan et al., 1988; Potter, 1990).

The median of K_{br} was higher for April than for October, as it had a lower E_a than the October. For October, the upper limit of K_{br}, which was about 6.0 mm/h with a 90% confidence limit, matched nearly the lower limit of K_b under the same confidence limit. Further, the distribution of K_{br} was almost the same as K_b with a reduction of about 3.0 mm/h and 2.0 mm/h in the median values for October and April, respectively.

The role of cover further reduced K_{sat} as the median of the $K_{e\text{-}nr}$ values was less than that for K_{br}. The added cover inhibits infiltration. When compared to K_b, the reduction in the median values of $K_{e\text{-}nr}$ was about 7 mm/h and 6.5 mm/h for the months of October and April, respectively. It is also important to note, that the shape of the distribution changed from bimodal to positively skewed. Thus the effects of cover can override the inherent soil properties which shaped both K_b and K_{br}. The total effective cover C_{TE} is one of the predominant factors that affect saturated hydraulic conductivity.

The median values for K_e increased about 5 and 3 mm/h for October and April, respectively, when compared to median values of $K_{e\text{-}nr}$. This increase in K_e shows the importance of single storm events in estimating the saturated hydraulic conductivity (Nearing et al., 1996; Elhakeem and Papanicolaou, 2012). Additionally, the shape of the K_e histograms show near symmetric distribution with an increase in the saturated hydraulic conductivity when compared to $K_{e\text{-}nr}$.

The maps and histograms for K_{br}, $K_{e\text{-}nr}$, and K_e shown in Figs. 4 and 5 were normalized to K_b and these ratios are given in Fig. 6 for October, as an example. Similar distributions and trends for these ratios were also observed for April.

Fig. 6a shows the ratio K_{br}/K_b, which ranges between 0.47 and 0.72. For most of the areas within the watershed, a 30% reduction in K_b was observed due to changes in management practices and the kinetic energy of rainfall. This was also confirmed from the histogram, which shows a median of 0.67. K_{br} is always smaller than K_b. The baseline hydraulic conductivity, K_b, is the upper limit of K_{br} that can be approached only immediately after tillage, when random roughness is at its highest (i.e., $RR_{t\text{-}max}$). Higher levels of random roughness limit the crusting of the soil and its effects at reducing saturated hydraulic conductivity (Rawls and Brakensiek, 1985).

Fig. 6b shows the ratio $K_{e\text{-}nr}/K_b$, which ranges between 0.0 and 0.71. For most of the areas within watershed, a 50% reduction in K_b was observed due to changes in vegetation cover through the season. This emphasizes the important role of vegetation cover in reducing the infiltration rate due to rainfall interception. It can be seen from the histogram that $K_{e\text{-}nr}$ is always smaller than K_b as well, with a median of 0.14.

Lastly, Fig. 6c shows the ratio K_e/K_b, which ranges between 0.46 and 1.59. As can be seen from the histogram, K_e can be either smaller or larger than K_b, with a median of 0.75. Within the watershed, the K_e values which were larger than K_b were less than 5%. This is attributed to the rainfall effect on the porous structure of the surface soil at these locations.

4.3. Iowa K_{sat} dynamic maps

The coupled Rosetta-WEPP-GIS modeling framework was used to quantify K_{sat} dynamics across the state of Iowa. Maps of K_b, K_{br}, $K_{e\text{-}nr}$, and K_e are shown in Fig. 7.

The range of K_b values across the state spans three orders of magnitude, which is similar to the range of measured values from previous studies (e.g., Ferrer Julia et al., 2004; Papanicolaou et al., 2008, 2015). The K_b values follow the distribution of bulk soil properties across the state. These bulk properties are dictated by the parent material and resulting mineral skeleton of the soil (Oschwald et al., 1965). In Iowa, ~95% of the surface soils are formed from the three types of parent material: glacial till, loess, and alluvium. Furthermore, these parent materials are representative of the major landform areas in the state (Fig. 8; Ruhe, 1969).

The Des Moines Lobe and the Iowan Surface are the two landform areas in Iowa where the surficial parent material of the soil is dominantly glacial till (Prior, 1991). The soils in these areas are primarily loams and clay loams. The remaining landform areas (e.g., the Loess Hills and Southern Iowa Drift Plain) have loess or alluvium as the dominant surficial parent material and soils predominantly have higher silt and clay contents (e.g., silt loams; silty clay loams; silty clays.

Overall, the K_{br} values are lower than the K_b values as expected. The maximum K_{br} values (~20 mm/h) are almost an order of magnitude lower than the K_b values (~152 mm/h). Since the soil crusting and stability factors are also functions of bulk soil properties, namely of sand and clay content (Rawls and Brakensiek, 1985), the distribution of K_{br} in Iowa is similar to that of K_b for the same reasons mentioned above. For example, the Des Moines Lobe and the Iowan Surface are dominantly loamy soil had higher values (greater than 0.5) than the areas dominated by the silty loess.

However, K_{br} is also a function of E_a and RR_t, both of which vary temporally. These two parameters are dynamic and account for changes in management practices and climate conditions around the state over the different seasons.

The cumulative rainfall kinetic energy between May and October of 2007 (derived from mostly convective storms) was greater than that of November 2007 to April 2008, which seems reasonable considering the

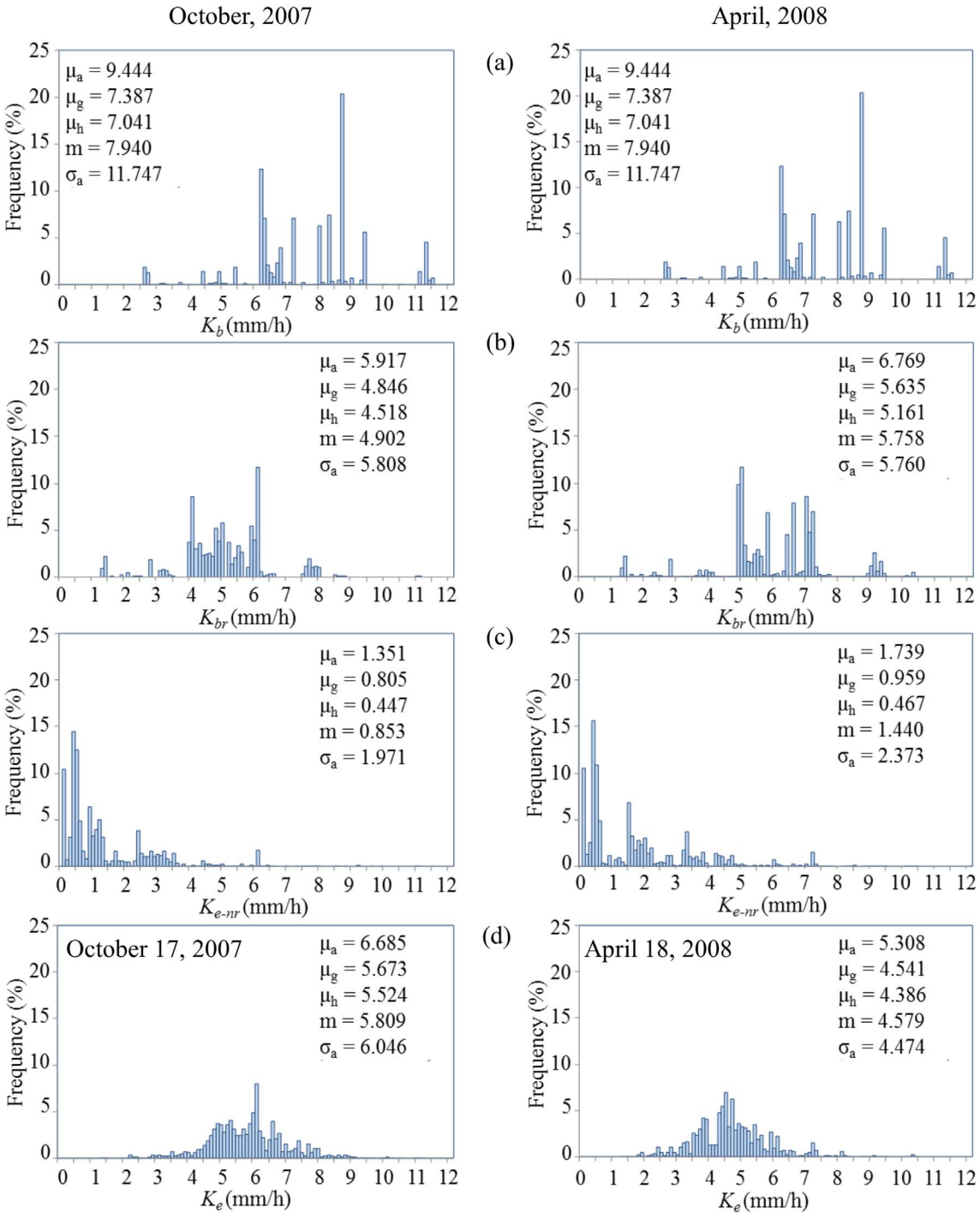

Fig. 5. Histograms of (a) K_b; (b) K_{br}; (c) $K_{e\text{-}nr}$; (d) K_e.

high intensity rains experienced in Iowa during the summer months. April had an overall higher K_{br} values than October because K_{br} is inversely proportional to E_a and the winter-spring in Iowa are generally characterized by lower precipitation intensities compared to summer-fall with the preponderance of high-intensity, convective rain storms. Nonetheless, the distribution of K_{br} in Iowa is similar to that of K_b because soil crusting and stability factors are also functions of bulk soil properties.

For both periods, $K_{e\text{-}nr}$ maps show lower values in the central part of the state of Iowa compared to the western and eastern parts, which reflect the differences associated with the management practices across the state and degree of soil disturbance for corn and soybean across the state (e.g., primary and secondary tillage). April also has higher $K_{e\text{-}nr}$ values than October.

For the single storm event of October 17, 2007, the K_e map shows higher values in the eastern part of the state of Iowa, while for the single storm event of April 18, 2008, the K_e map shows higher values in the eastern and western parts of the state. It can be noted that the maximum K_e value (~12 mm/h) is almost half that of the K_b value (~20 mm/h). This is attributed to the residue and leaf cover, which provide another barrier by intercepting the rainfall and preventing the direct infiltration of water into the soil. It can be seen from Fig. 7d that K_e has the largest variability across the state. More importantly, the distribution of K_e across the state is not dominated by intrinsic soil

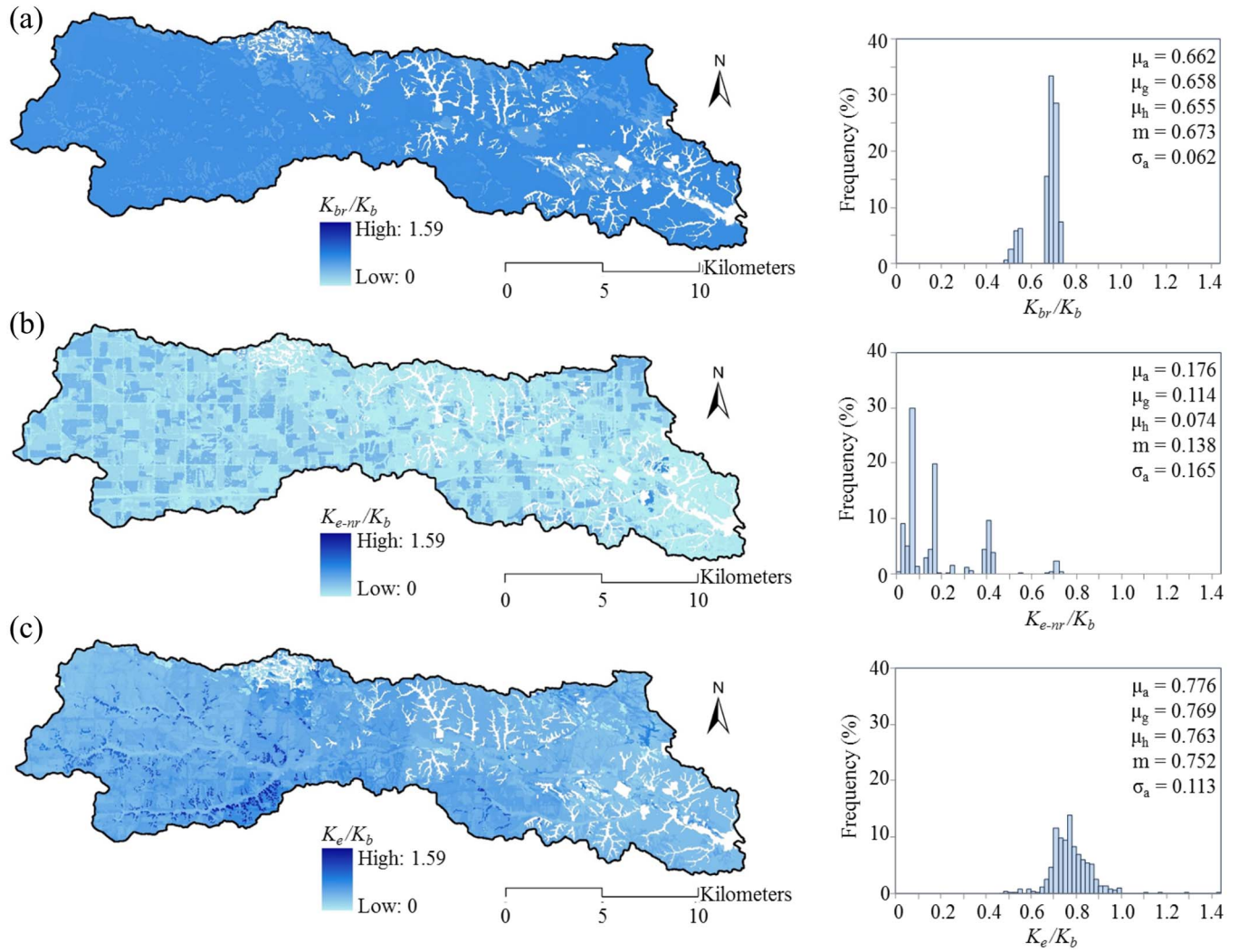

Fig. 6. Ratios of (a) K_b; (b) K_{br}; (c) $K_{e\text{-}nr}$; (d) K_e to K_b for October in Clear Creek.

properties and following the pattern of the major landform areas in the state like the cases of K_b and K_{br}. Thus, individual rainfall events strongly affect the distribution of K_{sat}.

K_e is linearly proportional to rainfall depth and the areas that received the highest rainfall during the two events (namely the eastern part of the state) had the highest K_e (Fig. 7d). Wischmeier (1966) has shown that positive correlation exists between K_e and rainfall depth. More importantly, the distribution across the state is no longer dictated by the soil properties following the trend of the major landform areas in the state. By removing the rainfall effects as in Fig. 7, one can see the connection to major landforms returns. Thus individual rainfall events strongly affect the distribution of K_{sat} across the state.

5. Conclusions

The main contribution of this work was a deeper understanding of K_{sat} dynamics over both space and time under different intrinsic properties and extrinsic factors through the use of a physically-based, modeling framework which considers different geographic, climatic, and land use data to quantify K_{sat}. The modeling framework integrated selected PTFs and watershed models with GIS modules. The framework was tested in the Clear Creek, IA watershed and verified with field measurements. It was then applied to the whole state of Iowa. The maps can be used as decision-making tools for agencies and policy makers.

Rosetta and WEPP provided the best estimates for K_b, K_{br}, $K_{e\text{-}nr}$, and K_e. The modeling framework helped visualize the data in the form of dynamic, geospatial maps. Two periods were selected to demonstrate K_{sat} dynamics in Clear Creek and the state of Iowa; specifically, May – October 2007 and November 2007 – April 2008, which corresponded to the pre-harvest and pre-planting conditions, respectively.

Histograms capturing the data for each K_{sat} type showed a unique pattern that does not change significantly with season. The histogram shape remained almost unchanged for each type of K_{sat}. The histograms of K_b and K_{br} were bimodal, while the histogram of $K_{e\text{-}nr}$ was positively skewed and the histogram of K_e was almost symmetric. Only the median magnitudes shifted due to seasonal changes in climate, cover, and management. K_b exhibited the highest median compared to other K_{sat} types. Both periods had higher median values for K_b, when compared to other K_{sat} types.

It was concluded that in intensively managed landscapes K_{sat} is a dynamic variable. The intrinsic soil properties incorporated in K_b do not reflect the degree of soil surface disturbance due to tillage and raindrop impact. Furthermore, vegetation cover must be incorporated in addition to the rainfall effect. Therefore, we suggest herein that K_e is the most representative saturated hydraulic conductivity in intensively managed landscapes because it accounts for the contributions of land cover and management, local hydropedology and climate condition, which all affect the soil porosity and structure and hence, K_{sat}.

One caveat in closing, it would be advisable to repeat this study in different regions, soil landform areas, and parent materials. The

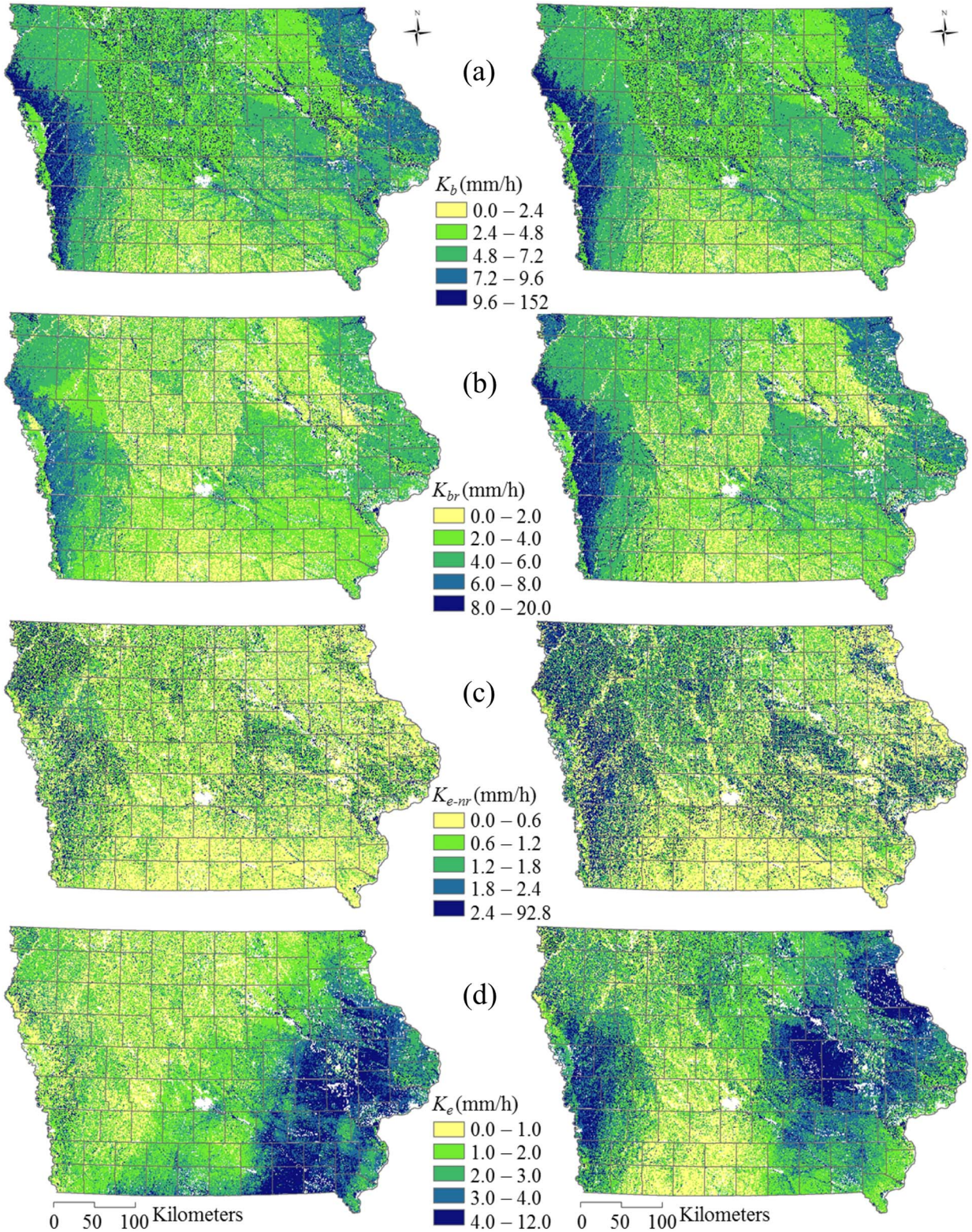

Fig. 7. Maps of (a) K_b; (b) K_{br}; (c) $K_{e\text{-}nr}$; (d) K_e for the state of Iowa.

applicability of the selected PTFs and watershed models used within this modeling framework may be limited to the state of Iowa, other Midwestern states, and other areas (e.g., Chinese Loess Plateau) having similar glacial derived soils, intensive management, and climatic conditions. Where arid or semi-arid conditions are ubiquitous, different PTFs and models may be needed. This exercise could ultimately contribute to the development of ratings for many of the soil interpretations incorporated into the National Cooperative Soil Survey and update the K_{sat} data stored in public soil databases.

Acknowledgements

This study was funded by the U.S. Department of Agriculture – Natural Resources Conservation Service and the National Soil Survey

Fig. 8. Major Landforms. In Iowa there are seven major landform with each one represented by a different color above. Each landform is characterized by a unique principal soil association.
From Prior (1991).

Center in Lincoln, NE (68-7482-10-507). This research is also partially supported by the NSF Grant # EAR-1331906 for the Critical Zone Observatory for Intensively Managed Landscapes (IML-CZO), a Multi-institutional collaborative effort.

References

Abaci, O., Papanicolaou, A.N., 2009. Long-term effects of management practices on water driven soil erosion in an intense agricultural sub-watershed: monitoring and modeling. Hydrol. Process. 23, 2818–2837.
Akaike, H., 1974. A new look at the statistical model identification. IEEE Trans. Autom. Control AC-19, 716–723.
Alberts, E.E., Laflen, J.M., Rawls, W.J., Simanton, J.R., Nearing, M.A., 1995. Soil component. In: Flanagan, D.C., Nearing, M.A. (Eds.), USDA-Water Erosion Prediction Project, Hill Slope Profile and Watershed Model Documentation. 10. USDA-ARS National Soil Erosion Research Laboratory, West Lafayette, IN, pp. 7.1–7.47 NSERL Report.
Alleto, L., Coquet, Y., 2009. Temporal and spatial variability of soil bulk density and near saturated hydraulic conductivity under two contrasted tillage management systems. Geoderma 152, 85–94.
Arnold, J.G., Srinivasan, R., Muttiah, R.S., Williams, J.R., 1998. Large area hydrologic modeling and assessment: part I model development. J. Am. Water Resour. Assoc. 34 (1), 73–89.
Ascough, J.C., Nearing, M.A., Flanagan, D.C., Livingston, S.J., 1994. Hydrologic and Erosion Calculations in the Water Erosion Prediction Project (WEPP) Watershed Model. Am. Soc. Agric. Bio. Eng. (94-2037).
Bosch, D.D., Onstad, C.A., 1988. Surface seal hydraulic conductivity as affected by rainfall. Am. Soc. Agric. Eng. 31 (4), 1120–1127.
Bozdogan, H., 1987. Model selection and Akaike's Information Criterion (AIC): the general theory and its analytical extensions. Psychometrika 52, 345–370.
Brakensiek, D.L., Rawls, W.J., Stephenson, G.R., 1984. Modifying SCS Hydrologic Soil Groups and Curve Numbers for Rangeland Soils. American Society of Agricultural Engineers (PNR-84-203).
Burras, C.L., McLaughlin, J.M., Wills, S.A., Barker, M., Brummer, E.C., 2005. Soil Carbon and Quality in Seymour and Clarinda Soil Map Units, Chariton Valley, Iowa. Final Report. Chariton Valley RC&D (ISU Project 400-41-71-4216).
Campbell, G.S., Shiozawa, S., 1994. Prediction of hydraulic properties of soils using particle-size distribution and bulk density data. In: Indirect Methods for Estimating the Hydraulic Properties of Unsaturated Soils. University of California, Riverside, CA, pp. 317–328.
Chang, Y., 2010. Predictions of Saturated Hydraulic Conductivity Dynamics in a Midwestern Agriculture Watershed, Iowa. MSc Thesis. The University of Iowa, Iowa City IA.
Cosby, B.J., Hornberger, G.M., Clapp, R.B., Gann, T.R., 1984. A statistical exploration of soil moisture characteristics to the physical properties of soils. Water Resour. Res. 20, 682–690.
Coulthard, T.J., Macklin, M.G., Kirkby, M.J., 2002. A cellular model of Holocene Upland River Basin and alluvial fan evolution. Earth Surf. Process. Landf. 27 (3), 269–288.
Dai, S., Shulski, M.D., Hubbard, K.G., Takle, E.S., 2016. A spatiotemporal analysis of Midwest US temperature and precipitation trends during the growing season from 1980 to 2013. Int. J. Climatol. 36, 517–525.
Dane, J.H., Puckett, W., 1994. Field soil hydraulic properties based on physical and mineralogical information. In: van Genuchten, W. (Ed.), Proceedings of the International Workshop on Indirect Method for Estimation Hydraulic Properties of Unsaturated Soils. Univ. of California, Riverside, CA, pp. 389–403.
Deb, S.K., Shukla, M.K., 2012. Variability of hydraulic conductivity due to multiple factors. Am. J. Environ. Sci. 8 (5), 489–502.
Dermisis, D., Abaci, O., Papanicolaou, A.N., Wilson, C.G., 2010. Evaluating grassed waterway efficiency in southeastern Iowa using WEPP. Soil Use Manag. 26, 183–192.
Dideriksen, R.O., LaVan, M.R., Norwood, K.K., Steckly, S.R., Steele, J.E., 2007. Soil Survey of Iowa County. USDA-NRCS, Iowa.
Diiwu, J.Y., Radar, R.P., Dickinson, W.T., Wall, G.J., 1998. Effect of tillage on the spatial variability of soil water properties. Can. Agric. Eng. 40 (1), 1–7.
Eigel, J.D., Moore, I.D., 1983. Effect of rainfall energy on infiltration into a bare soil. In: Proc of ASAE conference on Advances in Infiltration, pp. 188–199 (Chicago IL).
Elhakeem, M., Papanicolaou, A.N., 2009. Estimation of the runoff curve number via direct rainfall simulator measurements in the state of Iowa, USA. Water Resour. Manag. 23 (12), 2455–2473.
Elhakeem, M., Papanicolaou, A.N., 2012. Estimation of runoff curve number and saturated hydraulic conductivity via direct rainfall simulator measurements. In: James, W., Irvine, K.N., Li, J.Y., McBean, E.A., Pitt, R.E., Wright, S.J. (Eds.), Storm and Urban Water Systems Modeling. Monograph 20. CHI Press, Guelph, Ontario.
Elhakeem, M., Papanicolaou, A.N., Wilson, C., 2017. Implementing streambank erosion control measures in meandering streams: design procedure enhanced with numerical modeling. Int. J. River Basin Manag. 15 (3), 317–327.
Ferrer Julia, M., Estrela Monreal, T., Sanchez del Corral Jimenez, A., Garcıa Melendez, E., 2004. Constructing a saturated hydraulic conductivity map of Spain using pedotransfer functions and spatial prediction. Geoderma 123, 257–277.
Flanagan, D.C., Ascough, J.C., Nicks, A.D., Nearing, M.A., Laflen, J.M., 1995. Chapter 1: overview of the WEPP erosion prediction mode. In: USDA Water Erosion Prediction Project: Hillslope Profile and Watershed Model Documentation. USDA-ARS (NSERL Report No. 10).
Flanagan, D.C., Gilley, J.E., Franti, T.G., 2007. Water Erosion Prediction Project (WEPP): development history, model capabilities and future enhancements. Am. Soc. Agric. Bio. Eng. 50 (5), 1603–1612.
Gupta, N., Rudra, R.P., Parkin, G., 1996. Analysis of spatial variability of hydraulic conductivity at field scale. Can. Biosyst. Eng. 48 (1), 55–62.
Hardie, M.A., Lisson, S., Doyle, R.B., Cotching, W.E., 2013. Evaluation of rapid approaches for determining the soil water retention function and saturated hydraulic conductivity in a hydrologically complex soil. Soil Tillage Res. 130, 99–108.
Highland, J.D., Dideriksen, R.I., 1967. Soil Survey of Iowa County. USDA-SCS, Des Moines Iowa.
Hu, X., Liu, L., Li, S., Cai, Q., Guo, J., 2012. Development of soil crusts under simulated rainfall and crust formation on a loess soil as influenced by polyacrylamide. Pedosphere 22 (3), 415–424.
Jabro, J.D., 1992. Estimation of saturated hydraulic conductivity of soils from particle size distribution and bulk density data. Trans. Am. Soc. Agric. Eng. 35 (2), 557–560.
Ju, W., Gao, P., Wang, J., Zhou, Y., Zhang, X., 2010. Combining an ecological model with remote sensing and GIS techniques to monitor soil water content of croplands with a monsoon climate. Agric. Water Manag. 97, 1221–1231.
Khan, M.J., Monke, E.J., Foster, G.H., 1988. Mulch cover and canopy effect on soil loss. Trans. Am. Soc. Agric. Eng. 31 (3), 706–711.
Leenhardt, D., Voltz, M., Bornard, M., Webster, R., 1994. Evaluating soil maps for prediction of soil water properties. Eur. J. Soil Sci. 45, 3–301.
Leij, F.J., Alves, W.J., van Genuchten, M.T., Williams, J.R., 1996. Unsaturated Soil Hydraulic Database, UNSODA 1.0 User's Manual. US Environmental Protection Agency.
Lin, H., 2003. Hydropedology: bridging disciplines, scales, and data. Vadose Zone J. 2, 1–11.
Lin, H., Zhang, W., Yu, H., 2014. Hydropedology: linking dynamic soil properties with soil survey data. In: Teixeira, W.G. (Ed.), Application of Soil Physics in Environmental Analyses: Measuring, Modelling and Data Integration. Progress in Soil Science. Springer International Publishing, Switzerland. http://dx.doi.org/10.1007/978-3-319-06013-2-2.
McCuen, R.H., 2003. Hydrologic Analysis and Design, third ed. Prentice Hall, Englewood, NJ.
Mohatny, B.P., 2013. Soil hydraulic property estimation using remote sensing: a review. Vadose Zone J. http://dx.doi.org/10.2136/vzj2013.06.0100.
Morin, J., Keren, R., Benjamini, Y., Benhur, M., Shainberg, I., 1989. Water infiltration as affected by soil crust and moisture profile. Soil Sci. 148 (1), 53–59.
Mudgal, A., Anderson, S.H., Baffaut, C., Kitchen, N.R., Sadler, E.J., 2010. Effects of long-term soil and crop management on soil hydraulic properties for claypan soils. J. Soil Water Conserv. 65 (6), 393–403.
Nearing, M.A., Liu, B.Y., Risse, L.M., Zhang, X.C., 1996. Curve numbers and Green-Ampt effective hydraulic conductivities. Water Resour. Bull. 32 (1), 125–136.
Oneal, B.R., 2009. Quaternary Stratigraphy and Pedology of Clear Creek Watershed in Iowa County, Iowa. M.S. Thesis. Iowa State University, Ames, IA.
Oschwald, W.R., Riecken, F.F., Dideriksen, R.I., Scholtes, W.H., Schaller, F.W., 1965. Principle Soils of Iowa. Iowa State Univ (Report No. 42. Ames IA).
Paleologos, E.K., Neuman, S.P., Tartakovsky, D., 1996. Effective hydraulic conductivity of bounded, strongly heterogeneous porous media. Water Resour. Res. 32, 1333–1341.
Papanicolaou, A.N., Elhakeem, M., Wilson, C.G., Burras, C.L., Oneal, B., 2008. Observations of soils at the hillslope scale in the Clear Creek Watershed in Iowa, USA. Soil Surv. Horiz. 49, 83–86.
Papanicolaou, A.N., Elhakeem, M., Wilson, C.G., Burras, C.L., West, L.T., Lin, H., Clark, B., Oneal, B.E., 2015. Spatial variability of saturated hydraulic conductivity at the hillslope scale: understanding the role of land management and erosional effect. Geoderma 243–244, 58–68.
Papanicolaou, A.N., Dermisis, D.C., Abban, B.K.B., Flanagan, D., Frankenberger, J., 2017a. Capturing the Dynamic Effects of Hillslope Heterogeneity on Overland Flow Using a Shock-capturing Numerical Scheme: A 1-D Approximation in the Downslope Direction. (Water Resources Research. In press).

Papanicolaou, A.N., Wilson, C.G., Tsakiris, A.G., Sutarto, T.E., Bertrand, F., Dey, S., Rinaldi, M., Langendoen, E.J., 2017b. Quantifying bank fluvial erosion rates using Photo Electronic Erosion Pins and in-situ flume: an improved methodology for estimating key properties of fluvial erosion. Earth Surf. Process. Landf. http://dx.doi.org/10.1002/esp.4138.
Patil, N.G., Singh, S.K., 2016. Pedotransfer functions for estimating soil hydraulic properties: a review. Pedosphere 26 (4), 417–430.
Potter, K.N., 1990. Soil properties effect on random roughness decay by rainfall. Am. Soc. Agric. Eng. 33 (6), 1889–1892.
Prior, J.C., 1991. Landforms of Iowa. Burr Oak Press, Iowa City, IA.
Rawls, W.J., Brakensiek, D.L., 1985. Prediction of soil water properties for hydrologic modeling. In: Proceedings of Symposium on Watershed Management. American Society of Civil Engineers, New York, pp. 293–299.
Rayburn, A.P., Schulte, L.A., 2009. Landscape change in an agricultural watershed in the U.S. Midwest. Landsc. Urban Plan. 93 (2), 132–141.
Rezaei Arshad, R., Sayyad, G.H., Mosaddeghi, M., Gharabaghi, B., 2013. Predicting saturated hydraulic conductivity by artificial intelligence and regression models. ISRN Soil Sci. 2013 (308159). http://dx.doi.org/10.1155/2013/308159.
Risse, L.M., Liu, B.Y., Nearing, M.A., 1995. Using curve numbers to determine baseline values of Green-Ampt effective hydraulic conductivities. Water Resour. Bull. 31 (1), 147–158.
Ruhe, R.V., 1969. Quaternary Landscapes in Iowa. Iowa State University Press, Ames, IA.
Safadoust, A., Mahboubi, A.A., Mosaddeghi, M.R., Gharabaghi, B., Voroney, P., Unce, A., Khodakaramian, G.H., 2012. Significance of physical weathering of two-texturally different soils for the saturated transport of *Escherichia coli* and bromide. J. Environ. Manag. 107, 147–158.
Salles, C., Poesen, J., Sempere-Torres, D., 2002. Kinetic energy of rain and its functional relationship with intensity. J. Hydrol. 257, 256–270.
Saxton, K.F., Rawls, W.J., Romberger, J.S., Papendick, R.I., 1986. Estimating generalized soil water characteristics from soil texture. Soil Sci. Soc. Am. J. 50, 1031–1036.
Schaap, M.G., 1999. Rosetta Version 1.0. U.S. Salinity Laboratory, ARS, U.S. Department of Agriculture, Riverside, CA.
Schaap, M.G., Leij, F.J., 1998. Database related accuracy and uncertainty of pedotransfer functions. Soil Sci. 163, 765–779.
Schaap, M.G., Leij, F.J., van Genuchten, M.T., 1998. Neural network analysis for hierarchical prediction of soil hydraulic properties. Soil Sci. Soc. Am. J. 62 (4), 847–855.
Schaap, M.G., Leij, F.J., van Genuchten, M.T., 2001. Rosetta: a computer program for estimating soil hydraulic parameters with hierarchical pedotransfer functions. J. Hydrol. 251, 163–176.
Schoeneberger, P.J., Wysocki, D.A., 2005. Hydrology of soils and deep regolith: a nexus between soil geography, ecosystems and land management. Geoderma 126, 117–128.
Shahin, M., van Orschot, H.L., Delange, S.J., 1993. Statistical Analysis in Water Resources Engineering. A. A. Balkema, Rotterdam, Netherlands.
Smith, R.E., 2002. Infiltration Theory for Hydrologic Applications. American Geophysical Union, Washington, DC.
Smith, R.E., Goodrich, D.C., Quinton, J.N., 1995. Dynamic, distributed simulation of watershed erosion - the Kineros 2 and Eurosem models. J. Soil Water Conserv. 50 (5), 517–520.
Sun, Z., Kang, Y., Jiang, S., 2010. Effect of sprinkler and border irrigation on topsoil structure in winter wheat field. Pedosphere 20 (4), 419–426.
Sutarto, T.E., Papanicolaou, A.N., Wilson, C.G., Langendoen, E.J., 2014. Stability analysis of semicohesive streambanks with CONCEPTS: coupling field and laboratory investigations to quantify the onset of fluvial erosion and mass failure. J. Hydraul. Eng. 140 (9). http://dx.doi.org/10.1061/(ASCE)HY.1943-7900.0000899.
Tietje, O., Richter, O., 1992. Stochastic modeling of the unsaturatedwater flow using autocorrelation spatially variable hydraulic parameters. Model. Geo-Biosph. Process. 1 (2), 163–183.
United States Department of Agricultural - USDA, 2008. Land Resource Regions and Major Land Resource Areas of the United States, the Caribbean, and the Pacific Basin, NRCS Major Land Resource Areas Explorer Custom Report. pp. 2008. http://www.cei.psu.edu/mlra/ (accessed July 31, 2008).
Vereecken, H., Maes, J., Feyen, J., 1990. Estimating unsaturated hydraulic conductivity from easily measured soil properties. Soil Sci. 149, 1–12.
Vieux, B.E., 2004. Distributed hydrologic modeling using GIS. In: Water Science Technology Series No. 48, 2nd ed. Kluwer Academic Publishers, Norwell Massachusetts.
Webster, R., Oliver, M.A., 2001. Geostatistics for Environmental Scientists. JohnWiley and Sons, Ltd., London, UK.
West, L.T., Abreu, M.A., Bishop, J.P., 2008. Saturated hydraulic conductivity of soils in the Southern Piedmont of Georgia, USA: field evaluation and relation to horizon and landscape properties. Catena 73, 174–179.
Wilson, C.G., Papanicolaou, A.N., Denn, K.D., 2012. Partitioning fine sediment loads in a headwater system with intensive agriculture. J. Soils Sediments 12 (6), 966–981. http://dx.doi.org/10.1007/s11368-012-0504-2.
Wischmeier, W.H., 1966. Relation of field-plot runoff to management and physical factors. Soil Sci. Soc. Am. J. 30, 272–277. http://dx.doi.org/10.2136/sssaj1966.03615995003000020036x.
Wosten, J.H.M., Lilly, A., Nemes, A., Le Bas, C., 1999. Development and use of a database of hydraulic properties of European soils. Geoderma 90, 69–185.